First principles reaction modeling of the electrochemical interface: Consideration and calculation of a tunable surface potential from atomic and electronic structure

Christopher D. Taylor,[1] Sally A. Wasileski,[2] Jean-Sebastien Filhol,[3] and Matthew Neurock[4,*]
[1]*Department of Materials Science and Engineering, PO BOX 400745 University of Virginia, Charlottesville, Virginia 22904, USA*
[2]*Department of Chemistry, CPO #2310, University of North Carolina at Asheville, Asheville, North Carolina 28804, USA*
[3]*Université Montpellier II, Bâtiment 15, CC014 Place Eugène Bataillon, 34095 Montpellier Cédex 5, France*
[4]*Department of Chemical Engineering, P.O. Box 400741, University of Virginia, Charlottesville, Virginia 22904, USA*
(Received 19 September 2005; revised manuscript received 17 January 2006; published 4 April 2006; publisher error corrected 13 April 2006)

A method for calculating and subsequently tuning the electrochemical potential of a half cell using periodic plane-wave density functional theory and a homogenous counter-charge is presented and evaluated by comparison to simulations which explicitly model the countercharge by a plane of ions. The method involves the establishment of two reference potentials, one related to the potential of the free electron *in vacuo*, and the other related to the potential of H_2O species far from the electrode. The surface potential can be specifically adjusted by the explicit introduction of excess or deficit surface charges in the simulation cell and the application of periodic boundary conditions. We demonstrate the absence of field emission from the electrode over the range of realistic electrochemical potentials covered and confirm that the method can explicitly determine reaction energies and adsorption geometries as a function of electrochemical potential. This latter point is most useful as it asserts the viability of this method to model electrochemical and electrocatalytical systems of academic as well as applied interest. We present two case studies. The first examines the changes in the structure of water at the metal interface as a function of potential over Cu(111). At cathodic potential, we observe the repulsion of H_2O from the interface and the rotation of the water dipole toward the interface. The second study follows the initial pathways for the electrocatalytical activation of methanol over Pt(111) and the corresponding potential dependent reaction energetics for these paths. The results demonstrate that changes in the electrochemical potential can significantly alter the reaction energetics as well as the overall reaction selectivity. While the case studies presented herein described equilibrium geometries (i.e., the ideal forms at zero kelvin), the method is also suitable for application to ensembles of thermally activated systems.

DOI: 10.1103/PhysRevB.73.165402 PACS number(s): 82.65.+r

I. INTRODUCTION

The structure and chemistry at the water/metal interface is critical for the performance of many biological, chemical and materials systems. An understanding of the structure and the properties of the aqueous-metal interface will likely be essential for the development of biologically compatible materials, electrocatalysts for fuel cells, corrosion-resistant surfaces, and electrochemically deposited electronic and magnetic metallic films. While well-defined spectroscopic characterization of surfaces via sum frequency generation, surface enhanced Raman spectroscopy, and diffuse reflectance infrared spectroscopy, as well as scanning tunneling microscopy, are beginning to provide atomic scale resolution[1,2] there is a strong need for theory to complement these experimental efforts and help provide a fundamental understanding of potential-dependent interfacial phenomena including changes in molecular structure,[3,4] chemisorption,[5,6] water activation,[7] and surface reconstruction.[8] Understanding the complex structure of the water-ion-adsorbate/metal interface and its dependence on potential has posed a major theoretical challenge for well over 100 years.[9] Recent computational and theoretical techniques have reached the stage whereby they can begin to complement experimental methods, and provide insight into the atomic scale features that control the chemistry at the aqueous/metal interface.[10–12] The ability to model electrochemical kinetic processes is also contingent upon a knowledge of elementary kinetic parameters which can be derived from atomistic models.[13]

A number of physical models for the electrochemical interface have been developed over the past 30 years. These models may be categorized according to the underlying methodology (i.e., Monte Carlo,[14–24] integral equation,[25–31] modified Poisson-Boltzmann,[32–36] density functional theory,[37,38] molecular dynamics,[39–59]or reaction-coordinate/potential energy surface formalisms[10,12]), or by the methods used to simulate each of the major components that comprise the electrochemical interface: the electrode, electrolyte, adsorbates, and the interactions between each. Detailed atomistic models of the electrode can be grouped into four categories: a hard (exponential or infinite step)[15,17,18,46,48] or soft (typically a 9-3 Lennard-Jones)[16,39–41,46,47,59,60] repulsive wall which may be optionally corrugated,[52,57–59] *ab initio* derived metal-water and metal-ion pair potentials,[42,43,50,55,56,61] quantum mechanics with periodic boundary conditions in which the electronic structure of the electrode is calculated in the field of either a continuum positive charge (jellium)[62–69] or ionic pseudopotentials,[10,12,49,51,53,54,70] and quantum mechanical valence electron cluster models.[71–82] The electrolyte has been modeled as either a distribution of point-charges or spherical ions embedded in a dielectric medium,[15,62,63] dipolar hard

sphere models,[18,39,64,65,67–69] or point-charge models for water (such as TIP4P, BJH, ST2, and SPC/E) [Refs. 14, 16, 39–43, 46–48, 50, 52, 55–59, and 61] or Born-Oppenheimer quantum mechanical models that incorporate the valence electronic structure of the solvent species.[10,49,51,53,54,70] In some cases, the electrochemical reaction center is modeled in the absence of solvent, with the exception of possibly one or two molecules.[71–82] Interactions between the electrode and electrolyte may be modeled using combinations of one or more of the following according to the models used: the method of images, particle-particle or particle-wall potentials, or electronic structure methods.

The overwhelming picture presented by these numerous theoretical approaches is that the metal-water interface, even at ambient temperatures, is highly organized. The combination of a compromised hydrogen bonding network at the solvent edge (the electrode wall acts as a "foreign object" inserted into the water network[83]) with often attractive metal-water interactions leads to the adoption of ordered structures near the surface, often referred to as "icelike" due to the prevalence of hydrogen-bonded ring structures (4–6 membered rings[23,61,70]) and an evident layering of the solvent close to the electrode as manifested in near wall peaks in the water density profile (see, for example, the Monte Carlo studies published in 1981 by Jonsson[18] and by Christou *et al.*[20] and the more recent molecular dynamics simulations by Price and Halley[49] and Halley *et al.*,[53] Izvekov *et al.*,[54] and Hartnig and Koper[59]). This latter point has also been demonstrated experimentally using x-ray reflectivity by Toney.[84] It has also been demonstrated, however, that although the time-averaged orientation is icelike, at any individual moment the water arrangements at the surface are completely "random".[23] There remains considerable discrepancy between the theoretical models regarding the preferred orientation of the water dipole with respect to the metal surface. This issue is yet to be resolved for even low coverage ice structures on various noble and transition metal surfaces.[85]

Although methods involving the solution of the full electronic structure are most time consuming, they are also considered to be most accurate, as fewer fundamental approximations are needed in the model, albeit at the expense of the scope (both spatial and temporal) of the simulation. Furthermore, the interfacial processes capable of discriminating between one preferred water orientation over another are highly dependent upon the balance between interactions with the solution and adsorption processes at the electrode. The energy scale of these processes (typically fractions of an electron volt)[86] can only be probed using quantum chemical methods. Already molecular dynamics simulations performed using *ab initio* methods have demonstrated striking differences with those performed using classical pair potentials. For example, the diminished density of water close to the interface and a sparsity of occupation of the atop sites observed by both Price and Halley[49] and Izvekov *et al.*[54] contrasts clearly with the close packing observed in the pair-potential simulations by Heinzinger and Spohr[87] and Spohr and Heinzinger.[88] On the other hand, the complete exploration of dynamic effects as a function of metal surface has yet to be explored in a consistent first-principles fashion.

The challenges to the quantum mechanical modeling of a complete donor/acceptor environment, such as that comprising a complete electrochemical cell, are described by Blumberger and Sprik,[89] and relate not only to size effects, but to the difficulty in calculating excited state properties within density functional theory. Furthermore, to describe a functioning electrochemical cell, one would have to adopt a non-equilibrium approach, such as is currently utilized in the description of molecular electronics, and subsequently extend this to the complete circuit of the working and reference electrode, the electrolyte phase, and the leads connecting the electrodes. Currently the modeling of such a system that crosses many orders of magnitude in spatial dimensions is unfeasible. It is more convenient, therefore, both theoretically and practically, to confine one's attention to the electrochemical half cell and to model the properties of the half-cell reaction at a specific potential or set of potentials. A brief review of quantum mechanical half-cell and related models is given below.

Half-cell systems containing a small, i.e., <10, number of atoms have been used extensively by Albu and Anderson,[71] Anderson,[72,73] Anderson and Albu,[74,75] Anderson and Debnath,[76] Anderson and Kang,[77] Anderson *et al.*,[78] Anderson and Ray,[79] Narayanasamy and Anderson,[80] Seong and Anderson,[81] and Sidik and Anderson[82] to consider various electrochemical processes. In these studies, researchers created an atomistic cluster representation of the reaction center, and varied both the reaction coordinates and electronic charge of the system to create potential surfaces for reactant and product states. From the intersection of these potential surfaces they can determine both the activation barrier and equilibrium potential. In addition to the neglect of hard-to-calculate thermodynamic quantities, such as the enthalpic pressure-volume term and the entropy, the neglect of solvent and extended surface interactions in the cluster model necessitates the use of parameters to approximate experimental equilibrium potentials.[80] A novel technique for including surrounding electrolyte via a Madelung sum has been recently published.[73] More recent work by Roques *et al.* has employed periodic boundary conditions to simulate electrochemical hydroxide adsorption upon an intact semi-infinite Pt_3Co slab.[12] The cluster model has also been applied to electrochemical problems by Crispin *et al.* to predict the extent of charge transfer occurring with chemisorption.[90]

Halley and Price pioneered much of the theoretical effort to utilize quantum mechanical calculations for the elucidation of atomic processes at the electrochemical interface, initially by solving for equilibrium dipole orientations using the jellium model for the metal[64,65,67] (see also the work of Schmickler and Henderson[69,91]), and then by developing tight binding molecular dynamics methods to study the orientation of water close to the interface and the corresponding behavior of the electrochemical potential.[11,49,53] Halley's work agrees with Toney's observations of full and partial organization of water at the electrode/electrolyte interface,[84] and has also demonstrated the need for an improved description of the electronic structure at the interface. A review of molecular dynamics approaches to modeling the electrode/electrolyte interface may be found in the papers by Spohr.[44,45]

Since the electric field at electrochemical interfaces is known to induce and control vibrational shifts of adsorbed

molecules (i.e., carbon monoxide),[92,93] some researchers[94–97] have modeled the electrochemically induced electric field by applying a homogeneous external field perpendicular to the surface within the simulation. This is straightforward for finite-cluster calculations, as an extra term can simply be added to the Hamiltonian. The field polarizes the charge in the cluster, producing positively and negatively charged surfaces, which subsequently influence surface adsorption properties. Within the cluster, the electron density of the metal atoms reorganizes and thereby screens the electric field, modifying the electrode's electrochemical potential. The cluster potential is tuned by changing the strength of the external field, but relating the electrochemical potential to a known reference is not straightforward.[98] This approach has also been adopted by Patritos and Paredes-Olivera[99] and Paredes-Olivera *et al.*,[100] who applied electric fields of varying strength to a model Ag(111) cluster and observed changes in the adsorption behavior of H_2O and OH species. More recently, Dominguez-Ariza *et al.* have proposed a coupled molecular dynamics and cluster model based on this approach to describe electron transfer in terms of Marcus theory.[101]

Nørskov *et al.* have recently examined a series of electrochemical processes on Pt(111) and other metal substrates.[102] The authors performed a series of calculations to determine the overall reaction energies for O_2 reduction in the gas phase on the metal surface. The calculations are subsequently corrected to begin to account for the influence of water. In addition, they established a reference to the H_2/H^+ electrochemical couple, and were thus able to calculate potential dependent reaction energies. The approach did not include variations in surface charge density caused by changes in electrochemical potential, but rather extrapolated energetics from the system at zero charge. More recent calculations, however, indicate that while the polarization is important in an absolute sense, the changes in reaction energies are not as sensitive provided the reactant and products have similar directional dipoles.[103] This claim can be directly evaluated using the method developed in this paper, which allows the explicit evaluation of reaction energies as functions of the applied electrochemical potential.

Lozovoi *et al.* have recently suggested the use of a potential reference and a homogeneous countercharge (in more recent work a countercharge of arbitrary shape has been applied) within the bounds of the electronic structure calculation.[104] By using this technique and corrections to the shape of the electrostatic potential within the periodic cell, they have modeled field-evaporation effects *in vacuo*.[105] The adoption of a periodic slab model for the electrode provides an improved description of the electronic structure, which is important for the correct calculation of electrode/adsorbate interactions. It has also been demonstrated to be important for modeling correct interfacial capacitances, due to the contribution of the Fermi distribution of the metal's electron tail.[64,65,67] The approach removes a number of the difficulties of using clusters, which have electronic and structural properties that are unique from bulk metal. These differences make it difficult to compare with experiments on well-defined model surfaces. A periodic slab model was adopted by Feibelman to consider the field dependence of surface diffusion on metal surfaces *in vacuo*.[106]

This idea was extended by Filhol and Neurock[107] to the case of electrode/electrolyte systems via the creation of two potential references—a vacuum state and an aqueous state. In addition to providing an enhanced description of the electrode, the use of the periodic model enables one to capture the constrained effects of condensed, rather than vapor phase water. Using the Filhol-Neurock technique, termed here as the *double reference* method, it is possible to apply an arbitrary charge to the metal. The method is described in detail in the following sections. Briefly, a net surface charge density is introduced to the electrode via the variation of the number of electrons available to the self-consistent calculation, and overall cell neutrality (a requirement of the periodic boundary conditions) is maintained by applying a homogeneous background charge, essentially mimicking the presence of a diffuse ionic distribution close to the interface. The resulting electric field that develops at the interface leads to a potential drop that can be quantified by comparing the Fermi level of the system with a reference potential established at some distance from the metal/water interface. Filhol has applied this system to the calculation of equilibrium potentials for water activation on Pd(111).[107] This method was also adopted by Cao *et al.* for simulation of electrochemical methanol dehydrogenation over an immersed Pt(111) electrode.[10]

In this paper we examine the methodology developed by Filhol and Neurock in detail and consider its ability to polarize the electrode/electrolyte interface, by comparison to the polarization obtained when an explicit counter-ion model is used. The meaning of cell capacitances and the potentials of zero charge calculated within this equilibrium, periodic model are contrasted to their experimental counterparts. We also consider the feasibility of this method to determine reaction energetics on model electrode surfaces and apply this to the study of the equilibrium water structure on Cu(111) and the thermodynamics controlling methanol activation on Pt(111).

II. THEORETICAL METHODS

The following sections address theoretical aspects of the double reference approach. Specifically, we discuss the introduction of two internal reference electrodes within the periodic slab metal/aqueous system, and the determination of the electrochemical free energy of the system. Last, computational details of the approach are considered.

A. Selection of a reference electrode

The electrochemical potential of an electrode/electrolyte interface is complex, determined by the chemical potential of various ions in solution, charge-transfer, and work-function effects of adsorption, the chemical composition of the electrode, the surface charge density, and even the molecular orientation and position of water and ions adsorbed at the interface. Since most of these effects manifest themselves by introducing some excess or deficit surface charge on the electrode, the simplest and most convenient way to model

electrochemical potentials in a direct fashion is by controlling the net charge density of the metallic slab. The remaining features can subsequently be included explicitly into the simulation in order to establish their effects. Tuning the net surface charge density can be readily accomplished in an electronic structure method by assigning an excess or deficit number of electrons n_e to the metal and a corresponding electronic charge $q=-n_e$ to the system with respect to neutrality. In order to avoid electrostatic energy divergence and maintain charge neutrality, a continuum countercharge of density $\rho_{bg}=-q/\Omega$, where Ω is the volume of the unit cell, must also be introduced across the entire unit cell, similar to the methods used by others for maintaining neutrality in charged isolated systems.[104,108–111] However, in the method described here, an aqueous environment is explicitly represented by the inclusion of a region of water molecules with near ambient density between the metal layers. The charged slab together with the compensating background charge polarize the water layer, creating an electrostatic potential profile that simulates the electrochemical double layer. While the continuum countercharge model has been shown to overscreen localized charges, such as arise in the modeling of charge defects in superconductors,[111,112] here it is employed in a physically meaningful way—that is, to simulate the double layer. In the simulation of charge defects in ionic crystals one typically does not wish to consider the interaction between the defect and its images, since often the charge and defect site are localized at some distance from one another. In the case presented herein, however, the countercharge in an electrochemical system is not discretely localized, but is delocalized according to the ionic distribution near the electrode. The electrode potential resulting from this polarization is related to the energy at the Fermi level $\phi'(f)$ but must be compared to a known potential within the calculation (i.e., an internal reference) to have any meaningful value. In band structure calculations of vacuum surfaces, this equates to a calculation of the work function $\phi(f)$, which is most commonly done[113,114] by referencing to the asymptotic electrostatic potential at some distance from the surface $\phi'(v)$.

$$\phi(f) = \phi'(f) - \phi'(v). \tag{1}$$

In the presence of water, and when the surface is charged, however, this procedure is not so simple. We therefore introduce the following twofold scheme.

In analogy to the procedure to determining the work function of uncharged slabs in vacuum, we introduce a vacuum layer within our simulation cell, such that it lies between the two sides of the solvated metal slab. This insertion is performed by cleaving the metal/aqueous system at the midpoint of the aqueous region and expanding the unit cell so that it contains a reasonably large vacuum region. This procedure allows the calculation of the work function of the metal/aqueous interface in a manner similar to that theorized by Trasatti,[115] and clearly related to that commonly utilized in vacuum interface/vapor-phase calculations in solid-state and surface physics. Work functions in the presence of adsorbates, such as H_2O, have also been calculated in this way.[116,117] Example plots of the planar averaged electrostatic potential versus distance profile for systems with and without the vacuum layer taken from a symmetrized metal/water interface are given in the upper and lower plots, respectively, of Fig. 1.

The system in Fig. 1 corresponds to a simulation cell containing two symmetric oxygen-bound $Cu(111)/H_2O_{(aq)}$ interfaces derived from a quasibilayer approach. The viability of structural models for water over metal surfaces based on the formation of bilayers has been amply demonstrated in the theoretical study by Michaelides *et al.*[85] The potential axis of the calculated distance-dependent potential curve (upper plot, Fig. 1), has been shifted such that the potential at the center of the vacuum layer $\phi'(v)$ is now $\phi(v)=0$ V (note the primed and unprimed notation for the unshifted (unreferenced) and shifted (referenced) potentials), thereby setting a vacuum reference point for the electrostatic potential. This is the first reference of the double reference approach. All points in the electrostatic potential profile $\phi'(z)$, including the middle layer of the metal slab with a potential of $\phi'(m)$, may now be shifted according to this reference point, to produce the referenced (unprimed) potentials.

$$\phi(z) = \phi'(z) - \phi'(v). \tag{2}$$

The electrostatic potential profile for the metal-aqueous system *without* the vacuum region can also be referred to an absolute potential, by adjustment of the metal slab potential in this calculation $\phi'_0(m)$, where the subscript 0 indicates the uncharged calculation without vacuum, such that the two profiles are aligned at this point

$$\phi_0(m) = \phi(m) = \phi'(m) - \phi'(v). \tag{3}$$

This correction allows us to reference the uncharged calculation to the vacuum level, by assuming that the electrochemical potential of the metal electrode is unchanged between the vacuum cleaved and nonvacuum cleaved cases. Under this assumption, we may subsequently shift all other potentials in the profile as follows:

$$\begin{aligned}\phi_0(z) &= \phi'_0(z) - \phi'_0(m) + \phi_0(m) \\ &= \phi'_0(z) - \phi'_0(m) + \phi'(m) - \phi'(v).\end{aligned} \tag{4}$$

The electrochemical potential of the half cell with reference to vacuum is then determined from the unreferenced Fermi potential, $\phi'_0(f)$ via

$$\phi_0(f) = \phi'_0(f) - \phi'_0(m) + \phi'(m) - \phi'(v). \tag{5}$$

It can be seen that this procedure follows naturally from the physical description of the absolute electrochemical potential offered by Trasatti.[115]

Since a variation in the electronic charge q leads to an electric field at the interface, a vacuum reference point cannot be established for the case when $-q \neq 0$. Instead, a portion of the aqueous region is fixed far from the electrode at its position in the uncharged, i.e., $q=0$, calculation while the rest of the system is relaxed in response to the applied charge. The electrostatic potential at this solution point $\phi_0(w)$ far from the electrode is then used as the second ref-

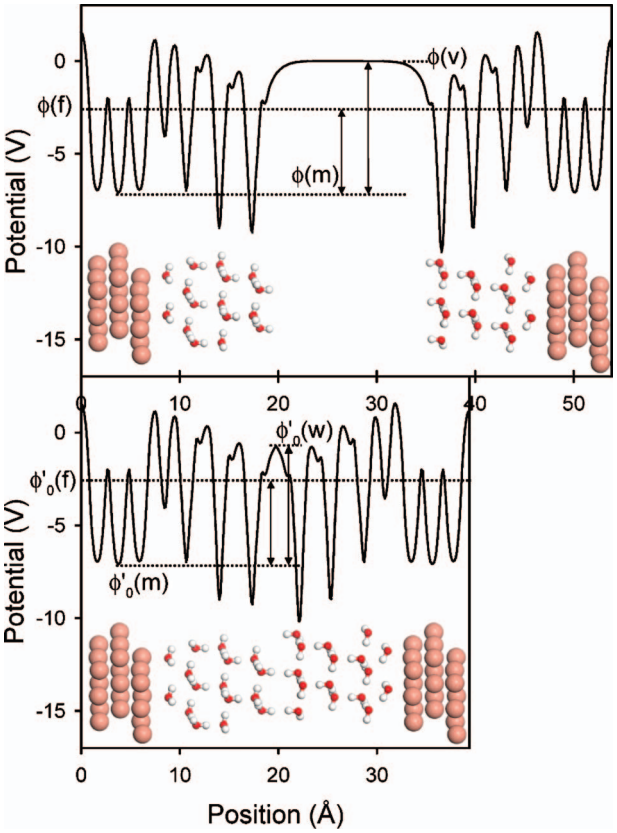

FIG. 1. (Color) A schematic diagram illustrating the electrostatic potential profile as a function of position across the normal axis of the unit cell. The system shown here contains two symmetric $Cu(111)/H_2O$ slab faces contained within the periodic simulation cell. The variables $\phi(v)$, $\phi(m)$, and $\phi(f)$ denote the position of reference, bulk metal, and Fermi potentials for the double reference model and are explicitly defined in the text. Top: The slab/water system shown in its elongated form due to the insertion of a vacuum reference electrode $\phi(v)$. Bottom: The closed unit cell containing the solvent phase reference electrode $\phi_0'(w)$, the bulk metal potential $\phi_0'(m)$, and the Fermi potential $\phi_0'(f)$.

erence point. The potential at all other positions, including the Fermi potential ϕ_f' is then shifted according to this second reference point

$$\phi_q(z) = \phi_q'(z) - \phi_q'(w) + \phi_0(w), \tag{6}$$

$$\phi_q(f) = \phi_q'(f) - \phi_q'(w) + \phi_0(w). \tag{7}$$

In all cases, charged and uncharged, the corresponding absolute potential $\phi_q(f)$ can be referenced to find a potential versus the normal hydrogen electrode (NHE) U_q by subtracting the work function for the $H_2/H+$ couple on Pt in standard conditions[118]

$$U_q/\mathrm{V} = -4.8 - \phi_q(f)/\mathrm{eV}. \tag{8}$$

Although the value 4.8 V has been selected for this study, estimates of the absolute potential of the normal hydrogen electrode vary from 4.4 through to 4.8 V.[115,119–123] The value may also be determined self-consistently from first-principles calculations.

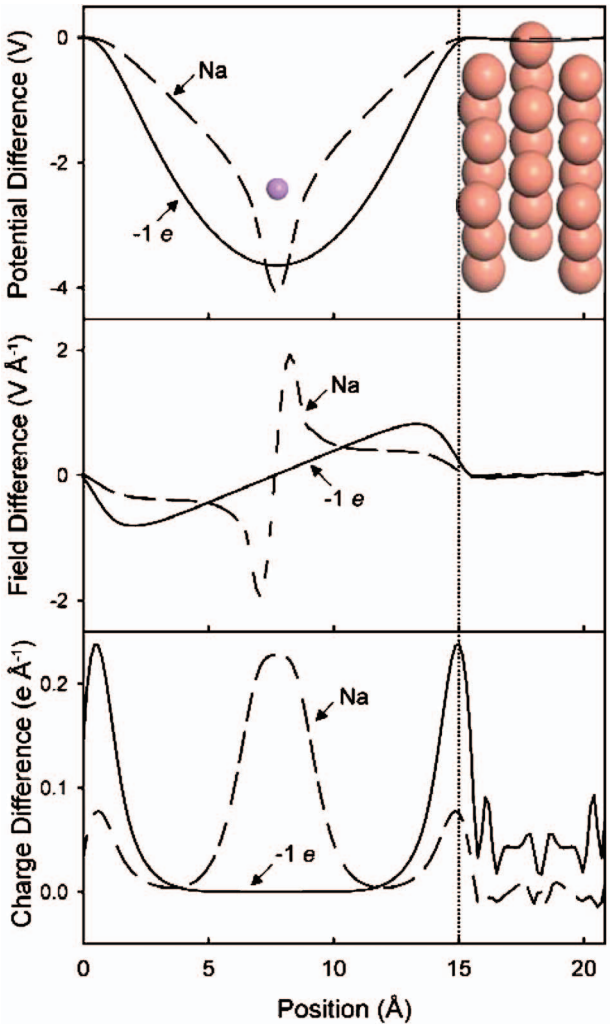

FIG. 2. (Color) The polarization of a bare Cu(111) slab by either a sodium ion pseudopotential at the outer Helmholtz plane (Na) or the use of a continuum countercharge (1e), is illustrated by comparing plots of the electrostatic potential (top), electric field (center), and the change in electron density (bottom).

B. Determination of the grand canonical free energy

The self-consistent energies calculated for the systems containing an excess charge and an homogeneous countercharge are not directly comparable between those systems containing varying amounts of charge. Furthermore, it would be ideal for electrochemical considerations to calculate energies that are directly comparable for systems at a constant potential. This imposes the requirement that the thermodynamic derivative of the system energy with respect to the electronic charge q must correspond to the electrochemical potential.

$$\frac{\partial E}{\partial q} = \mu. \tag{9}$$

Due to the inclusion of a homogeneous background charge density within the periodic calculation $\rho_{bg} = -q/\Omega$, however, the derivative acts on terms for both the electronic charge and the background charge, and Eq. (9) is not satisfied. Sepa-

rating the self-consistent energy E_{SCF} into terms for the charged metal/water interface, the interaction between the interface and the background, and the background, we may express the energy as, respectively,

$$E_{\mathrm{SCF}} = E_{\mathrm{MW}} + E_{\mathrm{MW/bg}} + E_{\mathrm{bg}} \tag{10}$$

and the derivatives as follows:

$$\frac{\partial E_{\mathrm{SCF}}}{\partial q} = \frac{\partial E_{\mathrm{MW}}}{\partial q} + \frac{\partial E_{\mathrm{MW/bg}}}{\partial q} + \frac{\partial E_{\mathrm{bg}}}{\partial q}. \tag{11}$$

The first term on the right-hand side is dependent upon the electronic charge alone, whereas the middle term is dependent on both the electronic charge and the countercharge, and the last term is dependent only on the countercharge. Decoupling the terms appropriately, and using the relation

$$E_{\mathrm{MW/bg}} = \int\int\int \rho_{\mathrm{bg}} V_{\mathrm{MW}} dxdydz, \tag{12}$$

where V_{MW} is the electrostatic potential arising from the metal slab and the water layer, in the absence of the background charge, it can be demonstrated that the derivative (11) is equal to

$$\frac{\partial E_{\mathrm{SCF}}}{\partial q} = \mu - \int\int\int V_{\mathrm{tot}}/\Omega dxdydz, \tag{13}$$

where V_{tot} is the total electrostatic potential arising from the metal/water interface and the background charge. The desired electrochemical energy E may be taken by integrating μ over the applied charge, where we use the dummy variable Q to represent the integration variable, and q represents the electronic charge of the system under consideration:

$$E = \int_0^q \mu dQ = E_{\mathrm{SCF}} + \int_0^q \left[\int\int\int V_{\mathrm{tot}}/\Omega dxdydz \right] dQ. \tag{14}$$

The term in brackets is the volume averaged electrostatic potential within the simulation cell $\langle \overline{V_{\mathrm{tot}}} \rangle$. Finally, a correction is also required to account for the different number of electrons present in each system, to yield the total grand canonical free energy of the cell (minus entropic and mechanical work contributions that require estimation from ensemble-based theoretical methods or available experimental data)

$$E_{\mathrm{free}} = E_{\mathrm{SCF}} + \int_0^q \langle \overline{V_{\mathrm{tot}}} \rangle dQ + \mu q. \tag{15}$$

C. Computational methods

Nonlocal gradient-corrected periodic density functional theory (DFT) calculations were carried out to determine the energetics, electronic structure, and potential for bare and aqueous-solvated Cu(111) and Pt(111) interfaces. The (111) surfaces were modeled using a three-layer periodic slab oriented in a face-centered cubic lattice arrangement with 27 metal atoms per unit cell repeating in a $p(3\times3)$ surface structure. Calculations with thicker slabs up to five layers showed changes in calculated energies to be on the order of 0.05 eV. The interatomic distances of the center metal layer were held fixed at the experimental bulk nearest neighbor distances (Pt 2.77 Å; Cu 2.56 Å),[124] while all other metal atoms were allowed to relax. For the aqueous systems, an icelike solvent structure was optimized for the $p(3\times3)$ repeat unit which consisted of 24 H_2O molecules oriented in eight hydrogen-bonded layers above the metal surface, completely filling the volume between the upper and lower slab surfaces. The icelike structure selected for the aqueous portion of the slab/water calculation was somewhat arbitrary since further evaluation of the large range of possible water arrangements and orientations, including a selection of suitable ensembles, is yet to be explored. For the $Cu(111)/H_2O$ system, the lattice vector perpendicular to the surface was set to obtain the ambient temperature liquid H_2O density of 1.0 g/mL.[124]

For the $Pt(111)/CH_xO_{(aq)}$ system, an optimal water density [0.86 g/mL, lower than that of ice, where ρ_{ice}=0.92 g/mL at 0 K and 1 atm (Ref. 124)] was established by expanding the lattice vector perpendicular to the surface plane to determine the lowest energy $Pt(111)/H_2O$ structure. When establishing an internal reference potential, either 15 Å [for the $Cu(111)/H_2O$ calculations] or 20 Å [for the $Pt(111)/CH_xO_{(aq)}$ calculations] of vacuum was inserted into the aqueous solvent layer halfway between the upper and lower slab surfaces, effectively bisecting the aqueous layer.

In order to test the double reference potential method described herein, we compare its predicted results for the potential and the field that form at the aqueous/metal interface with those determined by explicitly establishing an outer Helmholtz plane of ions at the metal/solution interface. More specifically, we directly modeled the charge transfer from a sodium atom which was placed inside the outer Helmholtz layer of the model $Cu(111)/H_2O$ interface. The sodium atom is anticipated to ionize, thus transferring its electron to the metal. This approach establishes a more naturally derived potential and field across the interface. This method is restrictive, however, in that only an integral number of electrons can be added to the small unit cell, whereas the homogeneous countercharge can take on nonintegral values, thus allowing for a continuum of surface charge densities to be considered. Nonintegral values for the electron count in periodic methods can be considered as whole electrons distributed over a number of simulation cells, and the derivative discontinuity at integral values is avoided since the energy derivative at the Fermi level of a metallic slab is continuous with electron occupation.[125,126] Furthermore the ability to determine the reference potential with reference to the uncharged case is obfuscated in the presence of ions or by the intrusion of an extra chemical species. Corrections due to the electric field of this ion, and the chemical potential of the ion would be required. Such corrections are not intractable, but depart from the simplicity and tenability of the method.

In order to model the polarization of the metal/water interface by an ion, we place a pseudopotential for the sodium ion halfway between the upper and lower slab surfaces either in vacuum or in the aqueous layer. For the latter system, the

solvent structure is held fixed to prevent the reorientation of water molecules to solvate the sodium ion. Calculations in which solvation shell relaxation was allowed led to the decomposition of water to hydroxides and H_2. A second effect of relaxation is that the O and H pseudopotentials relocate as the positions of the water molecules relax. This movement changes the detailed structure of the electrostatic potential profile, obfuscating the direct comparison between the polarized and unpolarized calculations. For this reason the solvent structure was not relaxed after introduction of the sodium ion.

In the methanol case study, we examined the dehydrogenation pathways over Pt(111), by following the reaction of one CH_xO^* species adsorbed per unit cell at a surface coverage of 1/9 and solvated by 23 H_2O with the adsorbate and water molecules fully optimized to their equilibrium configuration. The optimized system thus corresponds to a series of equilibrium structures at 0 K, again based on only one water ensemble out of the many complex arrangements of water that can occur at reaction conditions. The departing hydrogen atom from the dehydrogenation step is retained within the simulation cell, leading to a discontinuity in the local pH. In order to determine the pH dependence of the reaction thermodynamics, the proton can be coupled to a "virtual reservoir" that determines the chemical potential of protons in solution, which would contribute an additional term to the overall reaction energy. Such a procedure has been omitted in this work, and we focus only upon the discontinuous chemical changes that occur at the local reaction center. Further details of the study of CH_xO^* over Pt(111) are available in the recent publication by Cao *et al.*[10]

All calculations were performed using the Vienna *ab initio* simulation package (VASP) periodic density functional theory (DFT) code developed by Kresse and Furthmuller[127,128] and Kresse and Hafner.[129] The Kohn-Sham one-electron equations are solved in the DFT-generalized gradient approximation (GGA) approximation using the revised Perdew-Burke-Ernzerhof (RPBE) functional.[130,131] The electron density is described using plane waves with a kinetic-energy cutoff of 396.0 eV, determined by oxygen. The ion cores are described using ultra-soft pseudopotentials[132] developed using the PW91 (Ref. 133) correlation and exchange approximations. The Brillouin zone is sampled using a grid of $3\times3\times1$ Monkhorst-Pack special k points for all adsorbate structures.[134] Electronic self-consistent field (SCF) cycles are converged to 1.0×10^{-5} eV and the geometry was converged to 1.0×10^{-4} eV for quasi-Newton and conjugate-gradient optimizations. Partial occupancies of the wave function are allowed by including order-two Methfessel-Paxton smearing[135] at a width of 0.2 eV.

III. RESULTS AND DISCUSSION

In the following sections, a number of fundamental aspects of the double-reference method are discussed and compared to systems in which the surface potential is tuned by the inclusion of a minimal supporting electrolyte. This mode of polarization is addressed for conditions where the aqueous environment is both omitted (as in the work by Crispin *et al.*[90]) and included. Some treatment is also given to both the potential of zero charge and the capacitance measured using the double-reference method, since there is some inherent ambiguity in measuring the capacitance of a three-dimensional slab model. The discussion is followed by two case studies, which apply the double-reference method in considering the molecular structure and the adsorption of water at the aqueous Cu(111) interface and the potential-dependent reactivity of methanol dehydrogenation over Pt(111).

A. Comparisons between the polarizations of the inner layer induced by a continuum countercharge and an explicit plane of counterions

The well-established theoretical model of the electrochemical interface consists of a layer of excess electron density at the electrode surface balanced by solvated counter ions distributed starting from the outer Helmholtz plane (typically 3–10 Å from the electrode), and therefore resembles a capacitor with an induced electric field between the two charge planes.[136,137] Chemisorbed ions reside on the electrode surface within this layer. In the cases of a non-adsorbing electrolyte, the electrode will be "coated" by a thin inner layer of water molecules, beyond which the outer layer of ions begins. The physics of this diffuse ionic layer has been well-established following the theories of Gouy[138] and Chapman[139] developed using the Poisson-Boltzmann equation. The inner-layer solvent (in most cases, water) molecules have been shown using numerous simulations at a variety of levels of theory to fluctuate about a particular time-averaged orientation such that the potential drop across this inner layer is nonzero and linear.[49,53,140] In this section we evaluate and compare two different methods for polarizing this inner layer of water. In the first method, charge on the electrode is balanced by the inclusion of a uniformly dispersed continuum countercharge of the appropriate charge density to balance the charge on the electrode. In the second method, a plane of discrete ions is introduced using the sodium ion pseudopotential. The methods are compared by computing the electronic polarization induced at the interface using density functional theory. Solutions to Poisson's equation allow the comparison also of the electric field and electrostatic potential across the inner layer. We restrict ourselves only to the case where water is at the electrode, although there is no reason why, in principle, the model could not be extended to include the ion adsorption layer. Indeed, the flexibility to model various chemical and interfacial ensembles represents a key strength of this methodology.

The polarization of a Cu(111) slab with and without an aqueous environment is explicitly calculated by (a) adding an excess electron to the metal surface that is balanced by a continuum countercharge and (b) including a sodium atom, which is expected to donate an electron to the metal surface and leave a sodium ion in solution. In both cases, a formal surface charge density of 15.3 $\mu C/cm^2$ is introduced. Electrode polarization was assessed using three metrics: the electrostatic potential, the electric field, and the linear charge

density difference, plotted in the upper, middle, and lower segments, respectively, in Figs. 2 and 3 for the unsolvated and solvated systems. Solid and dashed lines refer to polarization induced by the continuum charge (a) and the sodium pseudopotential (b), respectively.

In the absence of a screening aqueous environment (Fig. 2), the induced polarization is significantly different for the two methods. The electrostatic potential follows a quadratic profile through the continuum countercharge (solid line), as expected from the classical solutions to Poisson's equation in a homogeneous medium, whereas the profile is more complex about the explicit ion layer (dashed line) due to the fact that the Na ion in the vacuum captures up to 76% of the excess electron. The preference for electron capture by the sodium ion is related to the competition between the electron affinity of Na^+ (−5.1 eV) (Ref. 124) and that of Cu(111) (calculated for the three layer slab in this work: −4.7 eV; experimental: −4.9 eV).[124] The lowering of the electrostatic potential in the vacuum outside the slab implies that caution must be applied, as a stationary state may evolve in which electron density can be localized in the vacuum. This is analogous to field emission which may occur in nonperiodic, nonequilibrium systems of electrified metal surfaces exposed to vacuum. The linear charge density difference plots in Fig. 2 indicate that the charge density here is not sufficient to create such a state. We estimate, from classical considerations, that the "field emission" in this system will occur at a limiting charge density of $-4\epsilon_0\Phi/L$, where L is the width of the vacuum layer and Φ is the work function of the metal. For the Cu(111) system discussed here, the limiting charge density is 11.1 $\mu C/cm^2$. This discrepancy of a higher calculated charge density than determined by the classical limit may be attributed to the delocalization of the charge across the first and second layers of the slab, which reduces the actual surface charge density to below the classical limit. Equilibrium field emission states in the periodic system were observed for higher surface charges and more elongated slab simulation cells, as the above equation implies.

The classical electric field induced at the surface by an applied formal surface charge density of 15.3 $\mu C/cm^2$ is 1.7 V/Å, following Poisson's equation. The density functional theory calculations performed in this work show much lower electric fields. By examining the electric field profile in Fig. 2, it can be seen that the continuum countercharge creates a maximum electric field of magnitude 0.81 V/Å, substantially greater than that induced by the sodium ion 0.34 V/Å. The maximum electric field is observed at a distance of 2.6 Å from the outermost metallic plane. Integrating the electron density over the interslab region indicates that the sodium ion pseudopotential captures 76% of the applied charge. An electric field with 24% of the classical field has a strength of 0.4 V/Å, compared to 0.24 V/Å observed here. The result is also reduced in the presence of the continuum countercharge due to the atomic and electronic structure of the conducting surface, and the linear dependence of the electric field throughout the continuum countercharge model (at 2.6 Å we may expect the electric field strength to be 1.1 V/Å without incorporating the effect of the tail of the electron distribution).

In an aqueous environment (Fig. 3), however, we see that the polarization of the interface induced by the sodium ion pseudopotential and the continuum countercharge become very similar due to the charge screening from the polarizable inner layer (which *reduces* the intensity of the continuum countercharge), and an endothermic electron affinity for aqueous Na^+ (thereby reducing the extent of electron capture and *increasing* the ion's efficacy to polarize the inner layer). The average electric field across the inner layer is therefore of similar magnitude for the two systems: 0.46 V/Å with the explicit ion method versus 0.42 V/Å for the homogeneously dispersed countercharge. The induced charge density difference is also comparable, but again greater for the continuum countercharge, since the sodium ion pseudopotential captures a portion of the excess charge (43%, down from 76% in the vacuum case), perhaps due to the unrelaxed solvation sphere. In both cases there is significant charging of the inner layer water matrix (around 30% of the charging electron is delocalized throughout the inner layer). *Ab initio* studies by Vassilev *et al.*,[51] as well as scanning tunneling microscopy imaging by Morgenstern *et al.*,[141] reveal that interfacial water is a weak conductor as the surface states couple with the molecular orbitals of H_2O. The pronounced extent of electron delocalization observed here (up to 7 Å) may be an artifact of the completely proton ordered water molecules in the icelike structure adopted herein. Future studies using molecular dynamics and disordered water configurations may illuminate this observation.

Alternatively, one may argue that this charge delocalization is a result of electron leakage to the water matrix via a field emission effect. To address this concern we have performed a calculation in which the formal charge density is +15 $\mu C/cm^2$, and thus field emission is prohibited (the slab is positively charged, the curve labeled "+1e" in Fig. 4). The charge distribution profiles are exactly symmetric between the positively and negatively charged cases. The polarization, therefore, is not a consequence of electron field emission into the positively charged background, but rather is indicative of strong coupling between the inner layer H_2O and surface states.

The average value of the electric field across the aqueous interface, 0.44 V/Å (Fig. 3), may be divided into the classical free-space prediction of 1.7 V/Å to yield a value of 3.9 for the dielectric constant of inner layer water. Since the water molecules have not been allowed to relax between the uncharged and charged calculations due to the necessity of calculating the difference profiles in Figs. 2 and 3, this number should be compared with the high frequency dielectric constant,[142] $\epsilon_\infty = 3.2$, rather than the conventional dielectric constant of water at the interface which has been estimated to be from between 5 and 10.[1,140,143] Relaxation of the water geometry in response to slab charging leads to rotation of the water dipole (as described in Sec. IV), which helps to explain the higher values based on electrochemical estimates. We find that our value and the value for the high frequency dielectric constant are in reasonable agreement. The somewhat higher value obtained in our calculation may be due to the retention of charge by the polarizing medium, in addition to the nonclassical distribution of charge across the conducting slab (i.e., not all charge is localized on the surface, and thus the classical description of the induced field as $E_{\text{classical}} = \sigma/\epsilon_0$ will overpredict the magnitude of the field, and hence

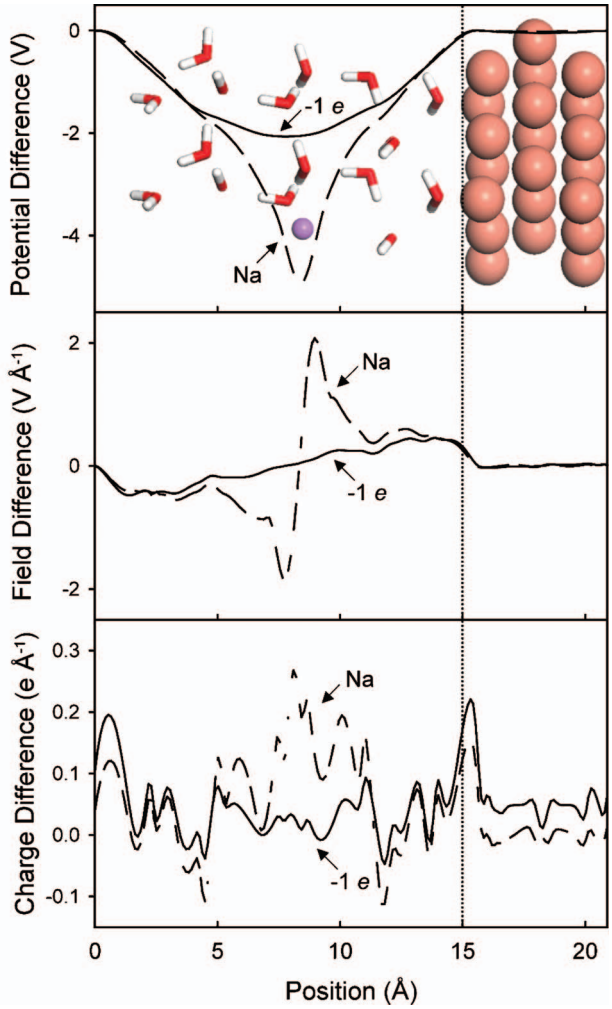

FIG. 3. (Color) The polarization of the $Cu(111)/H_2O$ interface by either a sodium ion pseudopotential at the outer Helmholtz plane (Na) or the use of a continuum countercharge (1e), is illustrated by comparing plots of the electrostatic potential (top), electric field (center), and the change in electron density (bottom).

the ratio $E_{obs}/E_{classical}=\epsilon_\infty$ will be higher than expected).

The similarity between the electric fields induced using the explicit ion and continuum polarization methods under aqueous conditions, therefore, leads us to expect that inner layer processes modeled by the continuum technique will coincide closely with real processes occurring in a double layer consisting of ions at the outer Helmholtz plane. This simplification is applicable to studies in which specific aspects of inner layer chemistry are being explored, and a nonadsorbing electrolyte can be assumed.

B. The uncharged reference potential and comparison to the potential of zero charge

The double reference method is predicated upon an initial calculation that determines the potential of the uncharged electrode/electrolyte interface. However, in the case where opposing sides of the slab represent two distinctly different interfaces, the question may be asked, "Which interfacial potential are we measuring, and is this the potential of zero

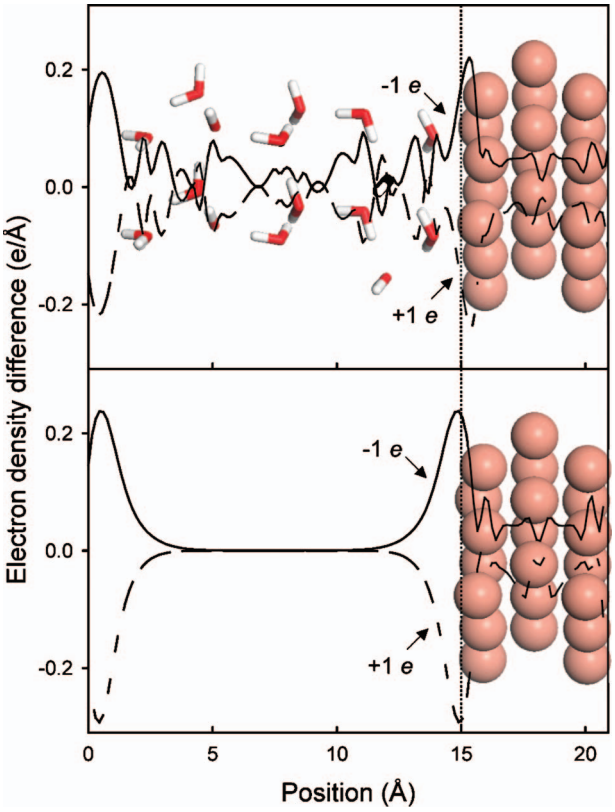

FIG. 4. (Color) The polarization of the charge density of the $Cu(111)/H_2O$ interface (top) and bare Cu(111) slab (bottom) is shown by presenting the electron density difference profile created by the difference between the charge density profile of the charged (+1e or −1e slab systems, corresponding to $\pm 15.3\ \mu C/cm^2$) and the neutral periodic slab system. Only the difference plots are shown.

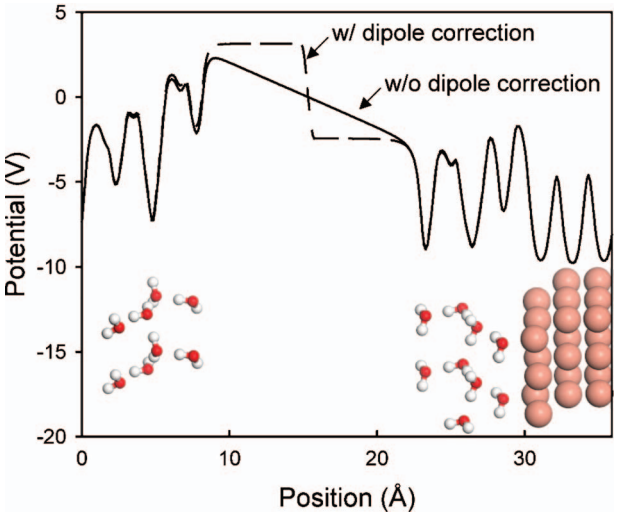

FIG. 5. (Color) The electrostatic potential profiles across the elongated "vacuum-reference" slab system, calculated either with or without a dipole correction are shown. The use of a dipole correction highlights the presence of two dissimilar work functions in operation due to the dissimilar slab face environments.

charge?" The "potential of zero charge" is a time-averaged macroscopic quantity over many dynamically changing interfacial configurations,[53,54,144] corresponding to the mean electrochemical potential observed when the electrode's net surface charge is determined by some means (for example, from an electrocapillarity curve) to be zero. The potential of zero charge, therefore, cannot simply be measured using a static, electronic structure calculation, but instead would require a large number of such calculations. The static potential of zero charge is often quite different from the measurable potential of zero charge due to the fluctuating orientation of water dipoles and other surface species, and we have made some effort to do this in a separate paper. By employing reference solvation structures of an appropriate orientation, however, a good estimate of the potential of zero charge can be obtained. We shall now demonstrate that the static potential of zero charge measured using the double reference method may be defined as the equilibrium (weighted mean) potential of a static system having two coupled interfaces with no net charge.

Consider the system portrayed in the top section of Fig. 4 and shown with a vacuum separated region in Fig. 5. An asymmetry exists between the two slab faces resulting from the completely proton-ordered icelike water structure taken from the geometry optimization performed on a relatively small slab (the difficulty in escaping such a structure is reminiscent of the Valleau and Gardner observation of "pathological anisotropy" in Monte Carlo simulations of liquid water[24]). Water molecules at the top of the surface are oriented upward with their hydrogen atoms pointing away from the surface. The proton-ordered structure creates an oppositely oriented water dipole at the opposing slab surface (hydrogen toward the surface). This is ultimately advantageous, however, as the averaged interfacial structure is therefore one of no net orientation with respect to the metal water interface, as may be expected for a dynamic liquid environment.

The coupling between these two slabs, and their resulting contribution to the measured electrochemical potential, was demonstrated by plotting the electrostatic potential across the slab/electrolyte/vacuum system when the dipole correction of Neugenbauer and Scheffler[145] is (dashed line) and is not (solid line) employed (Fig. 5). In this extreme example, the aligned orientation of water molecules in each of the two aqueous regions of the vacuum separated slab creates a ferroelectric effect[146] such that the work functions differ by approximately 6 eV. An electric field of magnitude 0.4 V/Å is thereby generated across the connecting vacuum region.

The apparent dilemma of having a system with two different Fermi levels is resolved by a consideration of the equilibration that occurs when the system is closed (i.e., when there is no vacuum layer). In this case charge must flow across the conducting slab in such a way that the work functions are equal (a counterfield is generated between the electrodes such that Φ_1 and Φ_2 in Fig. 5 are equal). The amount of charge required is determined by the difference in work functions multiplied by the capacitance of each interface. The equilibrium vacuum potential is therefore

$$\phi_v = \frac{C_1\Phi_1 + C_2\Phi_2}{C_1 + C_2}. \tag{16}$$

The double reference method in its current form implicitly assumes that the interfacial capacitances C_1 and C_2 are equal and therefore takes ϕ_v as the arithmetic mean of the two work functions [Eq. (16), Fig. 5]. This assumption (a consequence of taking the exact center of the interslab region as the vacuum reference electrode) is not as drastic as it may appear. The capacitances C_1 and C_2 in this case are derived from the response of the electronic wave function of the solvent to a change in potential about the interface (recall that the vacuum reference calculation is obtained from a single-point wave function calculation of the opened aqueous phase region with all atoms remaining frozen, thus there is no response from atomic motion here). For the cases considered in this paper, and previously by Filhol and Neurock[107] and Cao *et al.*,[10] both interfaces consist of proton ordered H_2O bilayers, and will therefore have a similar electronic response. Additionally, the interfaces are of similar width, comprising two water bilayers each, and therefore the capacitances C_1 and C_2 will be very close, if not the same. (Note: They will, of course, be slightly different because of the differences that arise due to the different chemi/physisorption interactions at the two dissimilar slab faces.) A quantitative argument, and more rigorous treatment of the vacuum potential, including the direct solution of Eq. (16) and an estimation of the error incurred when neglecting terms C_1 and C_2, is planned for a future paper.

Utilizing the assumption that $C_1 = C_2$, we determine that the potential of zero charge of the static $Cu(111)/H_2O$ model is +0.25 V (NHE). This is significantly higher than the most recent value of −0.70 V NHE determined by Lukomska and Sobkowski[147] for Cu(111) in perchloric acid (pH 5). These authors, along with others,[7,148–150] indicate that the potential of zero charge is highly sensitive to the adsorption of species derived from activation of water at the electrode, such as OH and H, as revealed by the pH dependence of their measurements, and consequently potentials in the range of −0.7 through to +0.7 V NHE have been reported. We therefore attribute the primary discrepancy between the calculated and experimental potential of zero charge values to the neglect of these ions directly in our simulation, and take the dynamic effect to be secondary. The inclusion of water activation effects, to produce hydrides and hydroxides over the electrode surface, for the determination of the potential of zero charge on Pd(111) is addressed in the recent paper by Filhol and Neurock[107] using the methodology described herein. It is anticipated that the potential of zero charge for $Cu(111)/H_2O$ may be dependent on the operation of a similar reaction chemistry, that changes the net charge density on the electrode surface.

As an aside, we can also demonstrate that the total differential capacitance of the coupled system is the sum of the differential capacitances on the two independent slab faces (now including the full effects of dipole rotation). This fact is necessarily true, for a change in the potential $d\phi$ each slab face must undergo a polarization by an amount of charge $d\sigma_1$ for interface 1 and $d\sigma_2$ for interface 2. The net charge must sum to the total system charge $d\sigma$. The partial charges upon each slab face are determined by their differential capacitance

$$d\sigma_1 = C_1 d\phi, \tag{17}$$

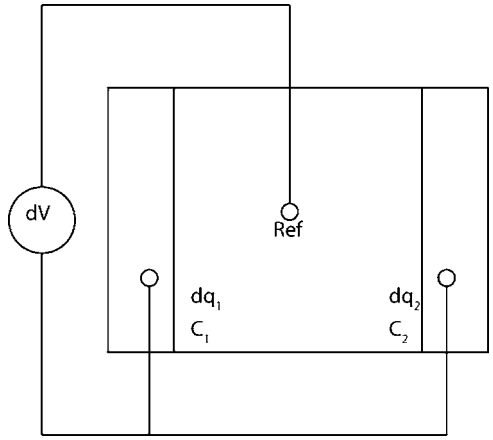

FIG. 6. Schematic indicating the effective parallel capacitor resulting from the use of the virtual reference electrode in the center of the aqueous region, and the two metallic electrodes resulting from the two sides of the periodic metallic slab.

$$d\sigma_2 = C_2 d\phi, \tag{18}$$

which sum to generate the total differential capacitance, $C_T = d\sigma/d\phi$. The two capacitors therefore act in parallel with respect to the virtual reference electrode we have introduced in the center of the aqueous region (Fig. 6).

The total capacitance may also be derived under the assumption of a classical response of the continuum countercharge and water dielectric to the slab charge density. Following Poisson's equation, and using atomic units

$$\nabla^2 \phi = \rho/\epsilon. \tag{19}$$

It is known that $\rho = -2\sigma/L$, where L is the axial length of the simulation cell, in the direction normal to the slab plane, which is approximately equal to the interslab spacing. From our previous section we have established a dielectric constant of 3.2. The electric field at the slab surface provides the boundary conditions for Poisson's equation over the dielectric

$$d\phi/dx(0) = \sigma/\epsilon, \tag{20}$$

$$d\phi/dx(L) = -\sigma/\epsilon. \tag{21}$$

Solving Poisson's equation gives

$$\phi(x) = -\sigma x^2/\epsilon L + \sigma/\epsilon x + \phi_0. \tag{22}$$

ϕ_0 is taken to be the electrostatic potential of the electrode. The potential at the midpoint of the aqueous region (the second reference potential), is therefore given by

$$\phi(L/2) = -\sigma L/4\epsilon + \sigma L/2\epsilon + \phi_0 = \sigma L/4\epsilon + \phi_0. \tag{23}$$

The differential capacitance is therefore given by $4\epsilon/L$. It is therefore essential to set the interslab spacing L to a reasonable size such that the potential does not change inordinately with the applied surface charge. For the range of examples considered in this work the predicted capacitance is between 5 and 10 μF/cm^2. The actual differential capacitance derived from the electronic structure is expected to differ from this classically derived due to the interaction between the surface charge density of the metal with the adsorbed water molecules and other near-surface species, and the response of the water dipoles as they relax to the applied charge density $d\sigma$.

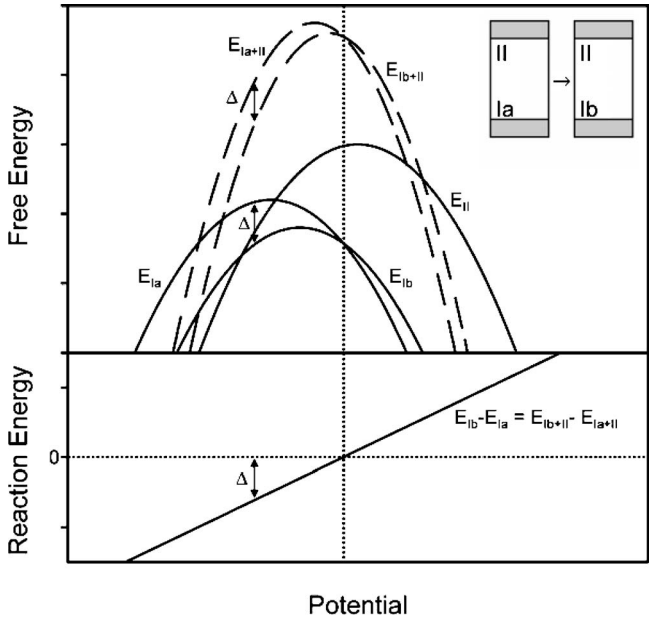

FIG. 7. A schematic of free energy versus potential (upper plot) for hypothetical periodic-slab calculations of the reaction Ia→Ib, participating at the lowermost slab face in the inset, is shown. The subscripts a and b indicate states at slab face I that are related by some physical or chemical change. Dashed lines $E_{\mathrm{Ia+II}}$ and $E_{\mathrm{Ib+II}}$, represent the calculated energy for the entire unit cell, consisting of contributions from the lower and upper surfaces (Ia and II) or (Ib and II) of the slab, as shown in the insert. Solid lines indicate hypothetical energy versus potential behavior for isolated Ia, Ib and II surfaces; E_{Ia}, E_{Ib}, and E_{II}, respectively. The reaction energy versus potential (lower plot, solid line) is not affected by the calculation periodicity, shown by the coincidence of the $E_{\mathrm{Ib}}-E_{\mathrm{Ia}}$ and $E_{\mathrm{Ib+II}}-E_{\mathrm{Ia+II}}$ curves, assuming that the environment of slab face II is constant.

C. Potential dependent reaction energies and decoupling of the slab faces

Although it is trivial to show that changes in energy related to changes in chemistry or water orientation at a given slab face can be decoupled from changes occurring at the other slab face, the justification for such a procedure is often nonintuitive. For this reason we shall spend some time demonstrating the separability of the two slab faces, and therefore the usefulness of this method in modeling chemical and physical changes systematically. In the following discussion, consider a slab with two opposing faces I and II. Consider also a physical or chemical change occurring at interface I, which may be represented by the reaction Ia→Ib, while the second slab interface remains inert. In Fig. 7 we have drawn schematic energy versus potential curves for such a process, in the cases where the slabs are both coupled (the curves $E_{\mathrm{Ia+II}}$ and $E_{\mathrm{Ib+II}}$) and decoupled (E_{Ia}, E_{Ib}, and E_{II}). The difference $E_{\mathrm{Ib+II}}-E_{\mathrm{Ia+II}}$ between the coupled curves is also given and shown to be equivalent to the uncoupled differ-

ence $E_{\mathrm{Ib}}-E_{\mathrm{Ia}}$ (i.e., the energy required to effect the change $\mathrm{Ia}\rightarrow\mathrm{Ib}$).

We have hitherto discussed the equilibration of work functions between the two isolated slabs such that the energy of the system [E_{free}, defined in Eq. (15)] conforms to the energy of the two-interface system as a function of some equilibrium potential ϕ. The total energy can also be described as the sum of the two independent interfacial energies. These energies are not completely independent, however, as there is the possibility that the two metal slab is polarized such that faces I and II have equal and opposite charge density. Thus for the coupled Ia+II and Ib+II systems described above

$$E_{\mathrm{Ia+II}}(0) = E_{\mathrm{Ia}}(\sigma_1) + E_{\mathrm{II}}(-\sigma_1), \tag{24}$$

$$E_{\mathrm{Ib+II}}(0) = E_{\mathrm{Ib}}(\sigma_2) + E_{\mathrm{II}}(-\sigma_2). \tag{25}$$

Despite the disparity in charge between the two slab faces, the electrochemical potential remains constant, since the two faces are in equilibrium with the same Fermi level having electrochemical potential ϕ. Hence, we may write

$$E_{\mathrm{Ia+II}}(\phi) = E_{\mathrm{Ia}}(\phi) + E_{\mathrm{II}}(\phi), \tag{26}$$

$$E_{\mathrm{Ib+II}}(\phi) = E_{\mathrm{Ib}}(\phi) + E_{\mathrm{II}}(\phi). \tag{27}$$

As shown in Fig. 7, each separate interface (Ia, Ib, and II) has its own thermodynamic dependence upon the potential (the solid curves E_{Ia}, E_{Ib}, and E_{II} in Fig. 7), although these dependencies are not readily separable. The summed curves $E_{\mathrm{Ia+II}}$ and $E_{\mathrm{Ib+II}}$ give rise to the coupled energy-potential curves indicated in Fig. 7 by the dashed lines. Following Eqs. (26) and (27) we see that, by keeping the potential-dependent chemical environment at one interface constant (that is the chemical environment of interface II in Fig. 7) we can calculate differences in energies between states at the other interface (such as the states Ia and Ib at interface I). Expressing this algebraically

$$E_{\mathrm{Ib+II}}(\phi) - E_{\mathrm{Ia+II}}(\phi) = E_{\mathrm{Ib}}(\phi) - E_{\mathrm{Ia}}(\phi). \tag{28}$$

Therefore the reaction energy for the reaction $\mathrm{Ia}\rightarrow\mathrm{Ib}$ (see the lower plot in Fig. 7) can be calculated as a function of the applied electrochemical potential, by calculating the energy functions $E_{\mathrm{Ia+II}}$ and $E_{\mathrm{Ib+II}}$ via the double reference method. The ability to infer such reaction energies as a function of electrochemical potential is of great importance for the study of reactions in electrocatalysis, as well as other natural processes, such as corrosion and biomolecular cell transport.

D. Application to water structure on Cu(111)

In the previous sections we have demonstrated that the double reference method allows for the assignment of an electrochemical potential to calculations performed in the constant charge ensemble. In this section we apply this method to probe the potential dependent reorganization of water over Cu(111) using density functional theory. An array of water molecules were distributed between two sides of a Cu(111) periodic slab with an interslab spacing of almost two nanometers. Slab charges of −15, −7.5, 0, +7.5, and +15 $\mu\mathrm{C/cm^2}$ were considered by adding or subtracting electronic charge from the interface. We focused on changes occurring only at the lower slab where the water molecules interact via the oxygen atom. Plotted in Fig. 8 (right axis) is the tilt angle of surface-bound H_2O versus the electrochemical potential as determined by performing a series of *ab initio* geometry optimizations at differing surface charge densities (between −15 and +15 $\mu\mathrm{C/cm^2}$) and calculating the electrochemical potential accordingly. The geometry used for the hydrogen bonded network of water within the simulation cell (Fig. 8, far right) parallels that of ice Ih,[151] with some deformations noted near the surface as the presence of the metal slab interrupts the hydrogen bonding network. The experimentally observed "flip-flop" mechanism of adsorbed water[152] is seen to apply, with the water dipole oriented 78° away from the surface normal at −1.4 V versus NHE, and rotating 20° toward the surface normal upon polarization to +1.3 V versus NHE. In the neutral slab, the water dipole is oriented at 66° away from the surface normal (or, alternatively, inclined 24° from the parallel/flat position) indicating a preference for Cu-O bonding. This is more inclined than both the 77° calculated for the orientation of adsorbed molecular water on a neutral Cu(111) cluster calculated at the MP2 level by Ruuska and Pakkanen[153] and the 75° calculated by Michaelides *et al.*[86] It is apparent that the presence of environmental solvent molecules are responsible for further inclining the water molecule to enhance the hydrogen bonding arrangement of interfacial water by directing the OH bonds towards the water bulk.

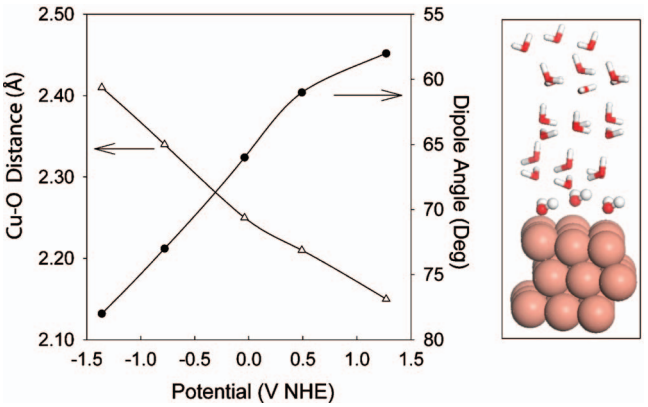

FIG. 8. (Color) Water dipole orientation, measured with respect to the surface normal such that an orientation of 0° indicates that the oxygen end is tilted directly toward the slab and 90° is a perfectly flat dipole orientation, and the copper-oxygen bond length are shown as a function of the electrochemical potential for water adsorbed at the $Cu(111)/H_2O$ interface (left). The atomic arrangement is also shown (right). Note that this diagram treats potential ranges over which the examined $Cu(111)/H_2O$ system may be metastable with respect to the formation of hydroxides, oxides or molecular hydrogen.

Plotted in Fig. 8 (left axis) is the change in the surface-oxygen bond distance for the interfacial H_2O, in which we clearly see the repulsion of surface H_2O species upon increasingly cathodic potentials. The Cu-O distance is 2.15 Å at +1.3 V versus NHE, and increases to 2.41 Å at −1.4 V

versus NHE. The centroid of these values (2.28 Å) is in good agreement with the Cu-O distance of 2.25 Å calculated for molecularly adsorbed water on a neutral Cu(111) slab by Michaelides *et al.*[86] The fact that the dipole angle changes more than the Cu-O distance between the molecular[86] and condensed phase (i.e., this work) calculations is in agreement with the higher mobility of the water protons compared to the oxygen atoms, as frequently observed in the molecular dynamics and numerical simulations cited in the introduction to this work.

There is also strong repulsion between the negative surface charge density ($-15\ \mu C/cm^2$) and the electron density on the oxygen atoms of the interfacial water molecules, as manifested in the increasing Cu-O bond distances as cathodic potentials are encountered. This result is consistent with the disappearance of adsorption spectra in the *in situ* truncated crystal rod experiments by Chu.[154] The protons on the water molecules, however, are attracted to the negatively charged surface. Such effects have been manifested in numerous molecular dynamics and other numerical simulations of the metal/water interface (see, for example, the molecular dynamics simulations of Price and Halley[49]). Yang, Yiacoumi, and Tsouris, in particular, observed this phenomenon in their Monte Carlo simulations[16] and note that the progressive change in dipole of their fluctuating-charge TIP4P-FQ water molecules is indicative of an enhanced potential for water dissociation at both anodic and cathodic potentials.

It is expected that water will reductively activate at cathodic potentials, leading to the evolution of molecular hydrogen,[155] and anodically activate at anodic potentials to form hydroxyl overlayers and both cuprous and cupric oxides.[7,150] At some of the potentials explored in this work, therefore, water is undoubtedly metastable. By varying the surface chemistry at this preferred slab face it is possible to calculate the reaction energies for these processes within this method, as a function of potential, and to therefore map out the regions of electrochemical potential "phase space" in which certain chemical environments are thermodynamically preferred. Such calculations have been performed and the results prepared for future publications.

E. Application to the dehydrogenation of methanol on Pt(111)

As an example of elucidating potential-dependent reaction energetics, as discussed above, we present a portion of our study of methanol dehydrogenation over Pt(111) surfaces, an important reaction for the chemistry of the direct methanol fuel cell. Complete details of this study, including a detailed comparison with the chronoamperometry and cyclic voltammagrams of Cao *et al.*[10] were recently published in their paper. For the example presented here, we focus solely on the first dehydrogenation step of methanol.

In an aqueous solution over platinum, dehydrogenation of the adsorbed methanol (CH_3OH^*) involves the heterolytic C-H or O-H bond cleavage to form an adsorbed hydroxymethyl (CH_2OH^*) or an adsorbed methoxy (CH_3O^*) species, respectively, and a solvated proton in solution. The reaction energies for aqueous-phase CH_3OH^*, $CH_2OH^*+H_{(aq)}$, and

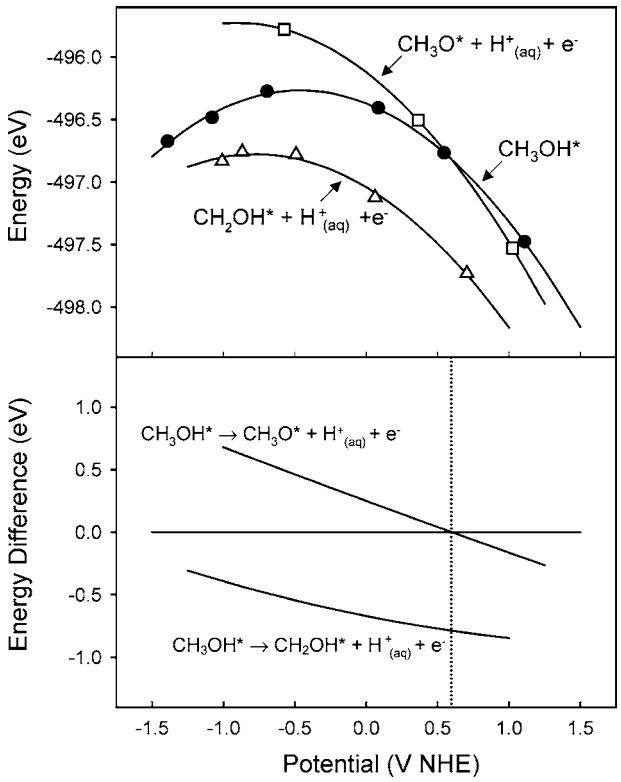

FIG. 9. To a close approximation, the energy varies quadratically with potential due to the continuum charge capacitor utilized in this work (top). The quadratic dependence of the energies of adsorbed hydroxymethyl, methanol, and methoxy are shown. Reaction energies for the two alternate pathways for methanol dehydrogenation are shown as a function of potential (bottom). Reaction energy curves are obtained from the difference of the individual product and reactant energy curves.

$CH_3O^*+H_{(aq)}$ systems are determined for various surface charges and plotted as a function of calculated potential as filled circles, open triangles, and open squares, respectively, in the upper portion of Fig. 9. Solid lines refer to a corresponding fit of the energy versus potential to a parabolic energy-potential curve.

The reaction equilibrium was then determined by calculating the free energies of the reactant and product states at each potential. The difference between these two free energies allowed the determination of the overall change in Gibbs free energy for the reaction, and was used to determine the reaction equilibrium at each potential. Additional terms and model features can be incorporated into future studies of the direct methanol fuel cell to allow for changes in the pH, coadsorbates, surface defects, etc., as models are expanded to increasingly approximate the complex operating conditions of a working environment.

The potential-dependent reaction energy is determined by subtracting the energy of the reactant curve from that of the product curve over the full range of potentials. The resulting reaction energy versus potential cure is plotted in the lower portion of Fig. 9. Cleavage of a C-H bond to form CH_2OH^* is exothermic over the range of -1 to $+1$ V versus NHE, becoming more exothermic toward more positive potentials. However, O-H cleavage to form CH_3O^* is endothermic at

negative potentials, becomes thermoneutral at $\sim +0.5$ V versus NHE (indicated by the vertical dotted line in Fig. 9) and is exothermic at more positive potentials, indicating significant potential dependence of the reaction mechanism. This example demonstrates the significant role of surface polarization in the reaction energetics and the corresponding reaction pathways, necessary to correctly predict the dehydrogenation chemistry.

IV. CONCLUSION

We have outlined a technique for calculating and subsequently controlling the electrostatic potential for a coupled two-interface system, and applied this method to the calculation of reaction energies relevant to two problems: one related to electrochemistry and the other to electrocatalysis. Increasing the surface electron density of a Cu(111) slab in contact with a condensed phase model of water was shown to repel the water molecules, both by increasing the metal-oxygen contact distance and rotating the direction of the water dipole. Decreasing the surface electron density was shown to have the opposite effect. The modification of the surface charge of a Pt(111) slab in contact with an aqueous "solution" of methanol, and the consequent change in potential, was shown to have consequences for the structure and reactivity of methanol over the slab face, including a change in the preferred dehydrogenation mechanism.

By comparing the polarization induced using the homogeneous background model to the polarization induced by a layer of explicitly modeled sodium ions, we show that similar fields and charge distributions are induced for the metal/water interface, but not for the metal/vacuum interface. The different response of the two models is attributed to the screening effect provided by the polarizable electronic structure of the solvent. Since computational limits constrain the extent to which the ionic nature of the electrolyte can be modeled completely, the homogeneous countercharge model appears to be a reasonable approach. Modifications to this general procedure have already been suggested, such as to model the countercharge distribution by a Gaussian model rather than as a uniform continuum.[156] These more complex models, however, have not yet been incorporated into a reference electrode model.

We have also demonstrated that arbitrary aspects of the presented model, such as the placement of a water reference electrode at the center of the interslab region, can lead to a significant dependence on the size of the model used, due to the quadratic dependence of the electrostatic potential throughout the continuum countercharge. A judicious choice of interslab spacing is necessary, therefore, to maintain a reasonable differential capacitance. The differential capacitance of the slab/water system is important since it is directly proportional to the curvature of the energy-potential function. Similarly an appropriate water structure must be adopted such that the measured "average" potential conforms to a physically reasonable result. In this case, the adoption of a completely proton ordered structure, while apparently irrelevant to any real system, led to a cancellation effect between the two separate interfacial dipoles and therefore an approximation to the completely proton disordered interfacial water structure. It is our opinion that the next step toward advancing the theories of water structure and polarization at the electrochemical interface is to treat ensembles of metal/water interfaces generated by *ab initio* molecular dynamics using the general methodology presented in this paper.

ACKNOWLEDGEMENTS

Financial support is gratefully acknowledged from the Army Research Office through the MURI Grant No. DAAD19-03-1-0169, and The Science of Localized Corrosion–A Center for Excellence for the Synthesis and Processing of Advanced Materials, K. Zavadil, project manager, Department of Energy Grant No. DE-FG02-00ER45825. We also acknowledge helpful discussions with Robert Kelly (Materials Science and Engineering, University of Virginia), and assistance with computations from John Fanjoy. Computer resources were provided by Pacific Northwest National Laboratories and the University of Virginia.

*Corresponding author. Email address: mn4n@virginia.edu

[1] D. M. Kolb, Angew. Chem., Int. Ed. **40**, 1162 (2001).
[2] D. M. Kolb and L. A. Kibler, Z. Phys. Chem. **217**, 1265 (2003).
[3] A. Bewick and K. Kunimatsu, Surf. Sci. **101**, 131 (1980).
[4] T. Iwasita and F. C. Nart, Prog. Surf. Sci. **55**, 271 (1997).
[5] J. Kunze, V. Maurice, L. H. Klein, H.-H. Strehblow, and P. Marcus, Corros. Sci. **46**, 245 (2004).
[6] B. J. Cruickshank, D. D. Sneddon, and A. A. Gewirth, Surf. Sci. Lett. **281**, 308 (1993).
[7] G. Niaura, Electrochim. Acta **45**, 3507 (2000).
[8] M. Wilms, P. Broekmann, C. Stuhlmann, and K. Wandelt, Surf. Sci. **416**, 121 (1998).
[9] J. O. M. Bockris and K. T. Jeng, Adv. Colloid Interface Sci. **33**, 1 (1990).
[10] D. Cao, G.-Q. Lu, A. Wieckowski, S. A. Wasileksi, and M. Neurock, J. Phys. Chem. B **109**, 11622 (2005).
[11] J. W. Halley, B. B. Smith, S. Walbran, L. A. Curtiss, R. O. Rigney, A. Sutjianto, N. C. Hung, R. M. Yonco, and Z. Nagy, J. Chem. Phys. **110**, 6538 (1999).
[12] J. Roques, A. B. Anderson, V. S. Murthi, and S. Mukerjee, J. Electrochem. Soc. **152**, E193 (2005).
[13] G. Brown, P. A. Rikvold, S. J. Mitchell, and M. A. Novotny, in *Interfacial Electrochemistry: Theory, Experiment, and Applications*, edited by A. Wieckowski (Marcel Dekker, 1999).
[14] K.-L. Yang, S. Yiacoumi, and C. Tsouris, J. Chem. Phys. **117**, 8499 (2002).
[15] L. Zhang, H. T. Davis, and H. S. White, J. Chem. Phys. **98**, 5793 (1992).
[16] K.-L. Yang, S. Yiacoumi, and C. Tsouris, J. Chem. Phys. **117**, 337 (2002).

[17] G. M. Torrie and J. P. Valleau, Chem. Phys. Lett. **65**, 343 (1979).
[18] B. Jonsson, Chem. Phys. Lett. **82**, 520 (1981).
[19] D. Boda, K.-Y. Chan, and D. Henderson, J. Chem. Phys. **109**, 7362 (1998).
[20] N. I. Christou, J. S. Whitehouse, D. Nicholson, and N. G. Parsonage, J.C.S. Faraday Symp. **16**, 139 (1981).
[21] J. Eggebrecht and P. Ozler, J. Chem. Phys. **93**, 2004 (1990).
[22] A. A. Gardner and J. P. Valleau, J. Chem. Phys. **86**, 4171 (1987).
[23] J. C. Shelley, G. N. Patey, D. R. Berard, and G. M. Torrie, J. Chem. Phys. **107**, 2122 (1997).
[24] J. P. Valleau and A. A. Gardner, J. Chem. Phys. **86**, 4162 (1987).
[25] A. Kramer, M. Vossen, and F. Forstmann, J. Chem. Phys. **106**, 2792 (1997).
[26] L. Blum and D. Henderson, J. Chem. Phys. **74**, 1902 (1981).
[27] A. A. Kornyshev, W. Schmickler, and M. A. Vorotyntsev, Phys. Rev. B **25**, 5244 (1982).
[28] F. Vericat, L. Blum, and D. Henderson, J. Chem. Phys. **77**, 5808 (1982).
[29] M. Vossen and F. Forstmann, J. Chem. Phys. **101**, 2379 (1994).
[30] G. M. Torrie, P. G. Kusalik, and G. N. Patey, J. Chem. Phys. **88**, 7826 (1988).
[31] S. L. Carnie and D. Y. C. Chan, J. Chem. Phys. **73**, 2949 (1980).
[32] C. W. Outhwaite and L. B. Bhuiyan, J. Chem. Soc., Faraday Trans. 1 **79**, 707 (1983).
[33] D. A. Cherepanov, Phys. Rev. Lett. **93**, 266104 (2004).
[34] L. B. Bhuiyan, C. W. Outhwaite, and D. Henderson, J. Chem. Phys. **123**, 34704 (2005).
[35] C. W. Outhwaite and M. Molero, Electrochim. Acta **36**, 1685 (1991).
[36] Z. Tang, L. E. Scriven, and H. T. Davis, J. Chem. Phys. **100**, 4527 (1994).
[37] J. Reszko-Zygmunt, S. Sokolowski, D. Henderson, and D. Boda, J. Chem. Phys. **122**, 84504 (2005).
[38] Y.-X. Yu, J. Wu, and G.-H. Gao, J. Chem. Phys. **120**, 7223 (2004).
[39] S. Senapati and A. Chandra, Chem. Phys. **231**, 65 (1998).
[40] S. Senapati and A. Chandra, J. Chem. Phys. **113**, 8817 (2000).
[41] A. Sonnenschein and K. Heinzinger, Chem. Phys. Lett. **102**, 550 (1983).
[42] E. Spohr, J. Phys. Chem. **93**, 6171 (1989).
[43] E. Spohr, J. Chem. Phys. **107**, 6342 (1997).
[44] E. Spohr, Solid State Ionics **150**, 1 (2002).
[45] E. Spohr, Electrochim. Acta **49**, 23 (2003).
[46] E. Spohr and K. Heinzinger, Electrochim. Acta **33**, 1211 (1988).
[47] C. Y. Lee, J. A. McCammon, and P. J. Rossky, J. Chem. Phys. **80**, 4448 (1984).
[48] M. Marchesi, Chem. Phys. Lett. **97**, 224 (1983).
[49] D. L. Price and J. W. Halley, J. Chem. Phys. **102**, 6603 (1995).
[50] J. I. Siepmann and M. Sprik, J. Chem. Phys. **102**, 511 (1995).
[51] P. Vassilev, R. A. van Santen, and M. T. M. Koper, J. Chem. Phys. **122**, 54701 (2005).
[52] K. Foster, K. Raghavan, and M. L. Berkowitz, Chem. Phys. Lett. **162**, 32 (1989).
[53] J. W. Halley, A. Mazzolo, Y. Zhou, and D. Price, J. Electroanal. Chem. **450**, 273 (1998).
[54] S. Izvekov, A. Mazzolo, K. VanOpdorp, and G. A. Voth, J. Chem. Phys. **114**, 3248 (2001).
[55] K. Raghavan, K. Foster, K. Motakabbir, and M. L. Berkowitz, J. Chem. Phys. **94**, 2110 (1991).
[56] I.-C. Yeh and M. L. Berkowitz, Chem. Phys. Lett. **301**, 81 (1999).
[57] P. S. Crozier, R. L. Rowley, and D. Henderson, J. Chem. Phys. **113**, 9202 (2000).
[58] P. S. Crozier, R. L. Rowley, and D. Henderson, J. Chem. Phys. **114**, 7513 (2001).
[59] C. Hartnig and M. T. M. Koper, J. Phys. Chem. B **108**, 3824 (2004).
[60] G. Barabino, C. Gavotti, and M. Marchesi, Chem. Phys. Lett. **104**, 478 (1984).
[61] A. Ignaczak and J. A. N. F. Gomes, J. Mol. Struct. **464**, 227 (1999).
[62] J. P. Badiali, M. L. Rosinberg, and J. Goodisman, J. Electroanal. Chem. Interfacial Electrochem. **130**, 31 (1981).
[63] J. Goodisman, J. Chem. Phys. **90**, 5756 (1989).
[64] J. W. Halley, B. Johnson, D. Price, and M. Schwalm, Phys. Rev. B **31**, 7695 (1985).
[65] J. W. Halley and D. Price, Phys. Rev. B **35**, 9095 (1987).
[66] O. K. Rice, Phys. Rev. **31**, 1051 (1928).
[67] D. L. Price and J. W. Halley, Phys. Rev. B **38**, 9357 (1988).
[68] W. Schmickler, J. Electroanal. Chem. Interfacial Electrochem. **150**, 19 (1983).
[69] W. Schmickler and D. Henderson, J. Chem. Phys. **85**, 1650 (1986).
[70] A. Klesing, D. Labrenz, and R. A. van Santen, J. Chem. Soc., Faraday Trans. **94**, 3229 (1998).
[71] T. V. Albu and A. B. Anderson, Electrochim. Acta **46**, 3001 (2001).
[72] A. B. Anderson, Surf. Sci. **105**, 159 (1981).
[73] A. B. Anderson, Electrochim. Acta **48**, 3743 (2003).
[74] A. B. Anderson and T. V. Albu, Electrochem. Commun. **1**, 203 (1999).
[75] A. B. Anderson and T. V. Albu, J. Am. Chem. Soc. **121**, 11855 (1999).
[76] A. B. Anderson and N. C. Debnath, J. Am. Chem. Soc. **105**, 18 (1983).
[77] A. B. Anderson and D. B. Kang, J. Phys. Chem. A **102**, 5993 (1998).
[78] A. B. Anderson, N. M. Neshev, R. A. Sidik, and P. Shiller, Electrochim. Acta **47**, 2999 (2002).
[79] A. B. Anderson and N. K. Ray, J. Phys. Chem. **86**, 488 (1982).
[80] J. Narayanasamy and A. B. Anderson, J. Phys. Chem. B **107**, 6898 (2003).
[81] S. Seong and A. B. Anderson, J. Phys. Chem. **100**, 11744 (1996).
[82] R. A. Sidik and A. B. Anderson, J. Electroanal. Chem. **528**, 69 (2002).
[83] L. J. Michot, F. Villieras, M. Francois, I. Bihannic, M. Pelletier, and J.-M. Cases, Comput. Geosci. **334**, 611 (2002).
[84] M. F. Toney, J. N. Howard, J. Richer, G. L. Borges, J. G. Gordon, O. R. Melroy, D. G. Wiesler, D. Yee, and L. B. Sorensen, Nature (London) **368**, 444 (1994).
[85] A. Michaelides, A. Alavi, and D. A. King, Phys. Rev. B **69**, 113404 (2004).
[86] A. Michaelides, V. A. Ranea, P. L. de Andres, and D. A. King, Phys. Rev. Lett. **90**, 216102 (2003).
[87] K. Heinzinger and E. Spohr, Electrochim. Acta **34**, 1849 (1989).
[88] E. Spohr and K. Heinzinger, Chem. Phys. Lett. **123**, 218 (1986).
[89] J. Blumberger and M. Sprik, J. Phys. Chem. B **109**, 6793 (2005).
[90] X. Crispin, V. M. Geskin, C. Bureau, R. Lazzaroni, W. Schmickler, and J. L. Bredas, J. Chem. Phys. **115**, 10493 (2001).
[91] W. Schmickler, J. Electroanal. Chem. Interfacial Electrochem.

150, 19 (1983).
[92] D. K. Lambert, J. Chem. Phys. **89**, 3847 (1988).
[93] J. D. Roth and M. J. Weaver, Langmuir **8**, 1451 (1992).
[94] M. Head-Gordon and M. Tully, Chem. Phys. **175**, 37 (1993).
[95] F. Illas, F. Mele, D. Curulla, A. Clotet, and J. M. Ricart, Electrochim. Acta **44**, 1213 (1998).
[96] M. T. M. Koper and R. A. van Santen, J. Electroanal. Chem. **476**, 64 (1999).
[97] S. A. Wasileski, M. T. M. Koper, and M. J. Weaver, J. Am. Chem. Soc. **124**, 2796 (2002).
[98] M. T. M. Koper, Curr. Top. Electrochem. **36**, 51 (2003).
[99] E. M. Patrito and P. Paredes-Olivera, Surf. Sci. **527**, 149 (2003).
[100] P. Paredes-Olivera, A. Ferral, and E. M. Patrito, J. Phys. Chem. B **105**, 7227 (2001).
[101] D. Dominguez-Ariza, C. Hartnig, C. Sousa, and F. Illas, J. Chem. Phys. **121**, 1066 (2004).
[102] J. K. Nørskov, J. Rossmeisl, A. Logadottir, L. Lindqvist, J. R. Kitchin, T. Bligaard, and H. Jonsson, J. Phys. Chem. B **108**, 17886 (2004).
[103] J. K. Nørskov (private communication).
[104] A. Y. Lozovoi, A. Alavi, J. Kohanoff, and R. M. Lynden-Bell, J. Chem. Phys. **115**, 1661 (2001).
[105] C. G. Sanchez, A. Y. Lozovoi, and A. Alavi, Mol. Phys. **102**, 1045 (2004).
[106] P. J. Feibelman, Phys. Rev. B **64**, 125403 (2001).
[107] J.-S. Filhol and M. Neurock, Angew. Chem., Int. Ed. **45**, 402–406 (2006).
[108] G. Macov and M. C. Payne, Phys. Rev. B **51**, 4014 (1995).
[109] J. M. Rosamilia, J. A. Abys, and B. Miller, Electrochim. Acta **36**, 1203 (1991).
[110] P. A. Schultz, Phys. Rev. B **60**, 1551 (1999).
[111] P. A. Schultz, Phys. Rev. Lett. **84**, 1942 (2000).
[112] J. Lento, J.-L. Mozos, and R. M. Nieminen, J. Phys.: Condens. Matter **14**, 2637 (2002).
[113] N. D. Lang and W. Kohn, Phys. Rev. B **3**, 1215 (1971).
[114] C. J. Fall, N. Binggeli, and A. Baldereschi, J. Phys.: Condens. Matter **11**, 2689 (1999).
[115] S. Trasatti, Electrochim. Acta **36**, 1659 (1991).
[116] S. Meng, E. G. Wang, C. Frischkorn, M. Wolf, and S. Gao, Chem. Phys. Lett. **402**, 384 (2005).
[117] S. K. Desai and M. Neurock, Phys. Rev. B **68**, 075420 (2003).
[118] F. T. Wagner, in *Structure of Electrified Interfaces*, edited by J. Lipkowski and P. N. Ross (VDH Publishers, New York, 1993).
[119] J. O. M. Bockris and S. D. Argade, J. Chem. Phys. **49**, 5133 (1968).
[120] R. Gomer and G. Tryson, J. Chem. Phys. **66**, 4413 (1977).
[121] H. Reiss and A. Heller, J. Phys. Chem. **89**, 4207 (1985).
[122] D. Tsiplakides and C. G. Vayenas, Solid State Ionics **152-153**, 625 (2002).
[123] D. Tsiplakides and C. G. Vayenas, J. Electrochem. Soc. **148**, E189 (2001).
[124] *CRC Handbook of Chemistry and Physics*, edited by D. R. Lide (CRC Press, Boca Raton, FL, 1992–1993).
[125] J. P. Perdew and M. Levy, Phys. Rev. Lett. **51**, 1884 (1983).
[126] J. P. Perdew, R. G. Parr, M. Levy, and J. L. Balduz Jr., Phys. Rev. Lett. **49**, 1691 (1982).
[127] G. Kresse and J. Furthmuller, Phys. Rev. B **54**, 11169 (1996).
[128] G. Kresse and J. Furthmuller, Comput. Mater. Sci. **6**, 15 (1996).
[129] G. Kresse and J. Hafner, Phys. Rev. B **47**, R558 (1993).
[130] J. P. Perdew, K. Burke, and M. Ernzerhof, Phys. Rev. Lett. **77**, 3865 (1996).
[131] J. P. Perdew, K. Burke, and M. Ernzerhof, Phys. Rev. Lett. **80**, 891 (1998).
[132] D. Vanderbilt, Phys. Rev. B **41**, R7892 (1990).
[133] J. P. Perdew, J. A. Chevary, S. H. Vosko, K. A. Jackson, M. R. Pederson, D. J. Singh, and C. Fiolhais, Phys. Rev. B **46**, 6671 (1992).
[134] H. J. Monkhorst and J. D. Pack, Phys. Rev. B **13**, 5188 (1976).
[135] M. Methfessel and A. T. Paxton, Phys. Rev. B **40**, 3616 (1989).
[136] D. C. Grahame, Chem. Rev. (Washington, D.C.) **41**, 441 (1947).
[137] N. F. Mott and R. J. Watts-Tobin, Electrochim. Acta **4**, 70 (1961).
[138] G. Gouy, J. Phys. Radium **9**, 457 (1910).
[139] D. L. Chapman, Philos. Mag. **25**, 475 (1913).
[140] J. O. M. Bockris, A. K. N. Reddy, and M. Gamboa-Aldeco, in *Modern Electrochemistry* (Kluwer Academic/Plenum Publishers, New York, 2000).
[141] M. Morgenstern, J. Muller, T. Michely, and G. Comsa, Z. Phys. Chem. **198**, 43 (1997).
[142] C. Zhang, K.-S. Lee, X.-C. Zhang, X. Wei, and Y. R. Shen, Appl. Phys. Lett. **79**, 491 (2001).
[143] J. O. M. Bockris and S. U. M. Khan, *Quantum Electrochemistry* (Plenum Press, New York, 1979).
[144] D. I. Dimitrov and N. D. Raev, J. Electroanal. Chem. **486**, 1 (2000).
[145] J. Neugebauer and M. Scheffler, Phys. Rev. B **46**, 16067 (1992).
[146] M. J. Iedema, M. J. Dresser, D. L. Doering, J. B. Rowland, W. P. Hess, A. A. Tsekouras, and J. P. Cowin, J. Phys. Chem. B **102**, 9203 (1998).
[147] A. Lukomska and J. Sobkowski, J. Electroanal. Chem. **567**, 95 (2004).
[148] M. L. Foresti, M. Innocenti, and G. Pezzatini, J. Electroanal. Chem. **434**, 191 (1997).
[149] S. Hartinger, B. Pettinger, and K. Doblhofer, J. Electroanal. Chem. **397**, 335 (1995).
[150] J. Kunze, V. Maurice, L. H. Klein, H.-H. Strehblow, and P. Marcus, J. Phys. Chem. B **105**, 4263 (2001).
[151] V. M. Nield and R. W. Whitworth, J. Phys.: Condens. Matter **7**, 8259 (1995).
[152] D. Henderson, Surf. Sci. Rep. **46**, 5 (2002).
[153] H. Ruuska and T. A. Pakkanen, J. Phys. Chem. B **108**, 2614 (2004).
[154] Y. Chu, Ph.D. dissertation, University of Illinois, 1997.
[155] Y. X. Chen, S. Z. Zou, K. W. Huang, and Z. Q. Tian, J. Raman Spectrosc. **29**, 749 (1998).
[156] A. Y. Lozovoi and A. Alavi, Phys. Rev. B **68**, 245416 (2003).